


Article

Design, Molecular Modeling and Synthesis of Metal-Free Sensitizers of Thieno Pyridine Dyes as Light-Harvesting Materials with Efficiency Improvement Using Plasmonic Nanoparticles

Mohamed E. Khalifa ^{1,*} , Abdulraheem S. A. Almalki ¹, Amar Merazga ² and Gaber A. M. Mersal ^{1,3}

¹ Department of Chemistry, Faculty of Science, Taif University, Taif 21974, Saudi Arabia

² Department of Physics, Faculty of Science, Taif University, Taif 21974, Saudi Arabia

³ Department of Chemistry, Faculty of Science, South Valley University, Qena 83523, Egypt

* Correspondence: mohamedezzat200@hotmail.com or mohamedezzat@tu.edu.sa; Tel.: +966-569846966

Received: 17 March 2020; Accepted: 14 April 2020; Published: 15 April 2020



Abstract: Considering the thiophene unit as an electron-rich heterocycle, it is investigated with the aim of elucidating its potential efficiency for solar cell application. With the introduction of active substituents such as COOEt, CONH₂ and CN into the thiophene segment, three novel thieno pyridine sensitizers (**6a–c**), based on donor-acceptor D- π -A construction, are designed and synthesized. The effect of the anchoring groups is investigated based on their molecular orbital's (MO's) energy gap (E_g). The electrostatic interaction between the synthesized dyes and metal nanoparticles, namely gold, silver and ruthenium, is believed to improve their performance as organic sensitizers. The dye-sensitized solar cells (DSSCs) are manufactured using the novel diazenyl pyridothiophene dyes, along with their metal nanoparticles conjugates as sensitizers, and were examined for efficiency improvement. Accordingly, using this modification, the photovoltaic performance was significantly improved. The promising results of conjugate (**6b**/AgNPs), compared with reported organic and natural sensitizers (J_{SC} (1.136×10^{-1} mA/cm²), V_{OC} (0.436 V), FF (0.57) and η ($2.82 \times 10^{-2}\%$)), are attributed to the good interaction between the amide, methyl, amino and cyano groups attached to the thiophene pyridyl scaffolds and the surface of TiO₂ porous film. Implementation of a molecular modeling study is performed to predict the ability of the thiophene moiety to be used in solar cell applications.

Keywords: tetrahydrobenzothiophenes; thienopyridine; HOMO-LUMO; organic sensitizers; dye-sensitized solar cells; metal nanoparticle; plasmonic

1. Introduction

Modern organic solar cells (OSC) are considered as third generation solar cells, as they were first fabricated by Grätzel et al. in 1991 [1]. They have remarkable advantages among potential renewable energy sources such as lower cost, simple fabrication and lower toxicity, and they are environmentally eco-friendly [2]. Dye-sensitized solar cells (DSSCs) of an organic nature are superior to metal-based sensitizers regarding the cost, environmental issues and higher molar extinction coefficients [3]. Typically, the common architect system (D- π -A) for DSSCs consists of a hydrophobic electron-rich donor π -conjugated bridge unit and a hydrophilic electron-deficient acceptor [4]. In this structure, the highest occupied molecular orbitals (HOMO) and the lowest unoccupied molecular orbitals (LUMO) are mainly localized around the donor and acceptor parts of the dye molecule, respectively [5]. This orientation favors the electron injection and slows down recombination between electrons in

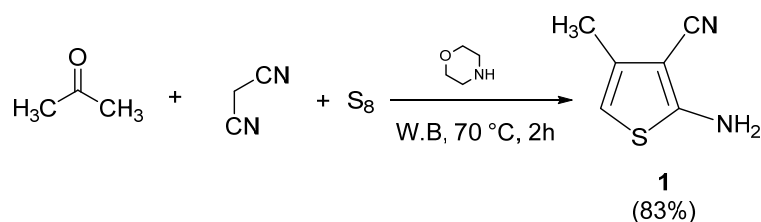
the TiO₂ photoanode conduction band (i.e., the semiconductor and oxidized molecules) through the anchoring/acceptor group adsorbed on its surface (i.e., a cyano, carboxylic or phosphonic group) [6,7]. The sensitizer is illuminated by the light; thus, the excited electrons will transfer from donor to acceptor terminals through the π -conjugation bridge and then inject into the conduction band. The design and mechanism of organic sensitizers for DSSCs have been explained in detail by Obotowo et al. [8]. The efficiency of a DSSC as light harvesting matter depends mainly on the nature and the amount of the adsorbed dye molecules on the photoanode [9,10] and the thickness of the photoanode as well [11]. To achieve the most optimized D- π -A dyes, they should be designed for broader absorption in the near IR region, minimizing the energy level mismatch between the oxidation potential of the dye's excited state and TiO₂ conduction band, and the HOMO and electrolyte as well, reducing the rate of charge recombination at the photoanode-electrolyte interface, prohibiting dye aggregation and increasing the stability of the DSSC [6]. Thiophene derivatives (e.g., bithiophenes [5], oligo thiophenes [5], aryl thiophenes [12] and aryl bithiophenes [13]) have attracted the attention of many researchers to synthesize donor-acceptor substituted π -conjugated systems, such as formyl π -conjugated systems, through cross-coupling/metalation followed by DMF quenching [5] and Vilsmeier-Haack-Arnold formylation reactions [13,14]. Plasmon resonance employing noble metals (i.e., Ag and Au) has been recently introduced to the DSSCs, where the metal nanoparticles' surface plasmon resonance phenomena are assumed to enhance their light harvesting efficiency [15]. It was reported that silver nanoparticles achieved light trapping in solar cells at a higher rate than that of other noble metals in visible range, due to their higher relative scattering efficiency [16]. In the light of the previous literature, it is of interest to design new, organic DSSCs of thienopyridyl thiophene dyes, identify their electrical characteristics and examine their utility in solar cell applications. In addition, the influence of the plasmonic resonance of different metal nanoparticles (namely gold, silver and ruthenium) on the redox properties has been investigated, aiming to enhance their light harvesting efficiency. Computational modeling study has also been performed in order to predict the reactive sites of the dyes' molecules and their ability to serve in the field of solar cell applications. Density functional theory (DFT) method exhibits outstanding explanation of the structural, spectral and electronic properties of the studied molecules [17–19]. The B3LYP calculation functional method has been chosen to predict the energetic, electronic and spectral properties for many molecules in high precision [20–22].

2. Results and Discussion

2.1. Chemistry

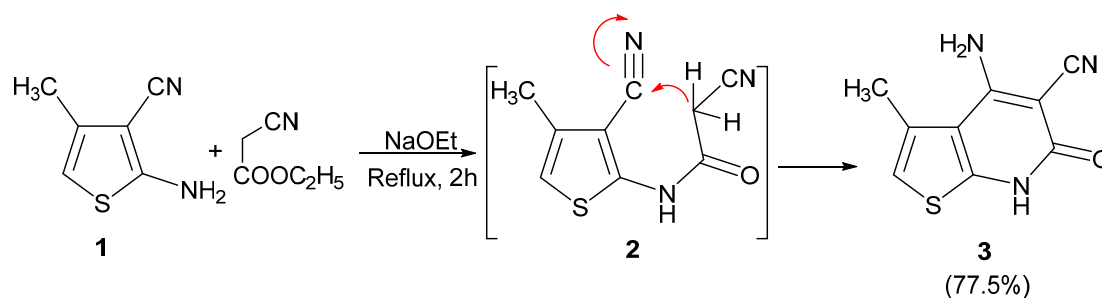
As a part of our continuous efforts for the synthesis of novel organic dye-sensitized solar cells [23–26], the thiophene nucleus has particularly attracted our attention. In this regard, we herein report the synthesis of novel scaffolds of diazenyl pyridothiophene derivatives (6a–c) as metal-free organic sensitizers.

The synthesis procedures are carried out using the 2nd version of Gewald strategy to achieve the final products starting from preparing the 2-amino-3-cyano-4-methylthiophene compound (1) [27]. As shown in Scheme 1, the acetone mixes readily with sulphur, malononitrile and the base catalyst (morpholine) to afford the target 2-aminothiophene derivative (1).



Scheme 1. Preparation of 2-amino-4-methylthiophene-3-carbonitrile (1).

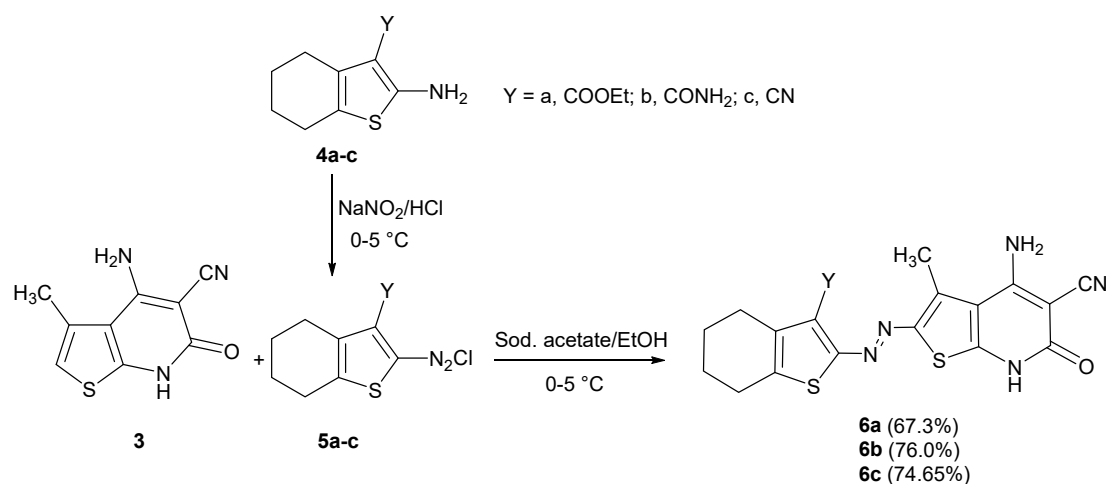
The mechanism of this reaction was proposed by Gewald [27]. The structure of the prepared starting compound (1) is secured by its micro and spectroscopic analyses and found to be in good agreement with the literature [28]. The cyclization of 2-amino-3-cyano-4-methylthiophene (1) with ethyl-cyanoacetate in the presence of sodium ethoxide affords the 4-amino-6,7-dihydro-3-methyl-6-oxothieno[2,3-*b*]pyridine-5-carbonitrile (3), as depicted in Scheme 2 [29].



Scheme 2. Synthesis of 4-amino-6,7-dihydro-3-methyl-6-oxothieno[2,3-*b*]pyridine-5-carbonitrile (3).

This reaction is assumed to proceed through formation of the non-isolable intermediate (2) followed by intramolecular cyclization to afford the cyclic pyridone (3) according to the Thorpe-Ziegler reaction mechanism [30].

On the other hand, preparation of 2-amino-4,5,6,7-tetrahydrobenzo thiophene derivatives (4a–c) was very interesting with the aim of coupling with the precursor compound (3) to collect the new products of (6a–c), as described in Scheme 3. Three components' reactions (cyclohexanone, active nitriles and elemental sulfur in ethanol) in the presence of a catalytic amount of morpholine undergoes Gewald synthesis to give the target products (4a–c) [31–34].



Scheme 3. Synthesis of thienopyridyl-azo-tetrahydrothiophene derivatives (6a–c).

Therefore, diazotization of 2-amino-4,5,6,7-tetrahydrobenzo[*b*]thiophenes (4a–c) in HCl and sodium nitrite gives the corresponding non-isolable diazonium salts (5a–c), which undergo coupling reactions with 4-amino-6,7-dihydro-3-methyl-6-oxothieno[2,3-*b*]pyridine-5-carbonitrile (3) in the presence of sodium acetate and ethanol to furnish the corresponding diazenyl pyridothiophene derivatives (6a–c) (Scheme 3).

The chemical structures of diazenyl pyridothiophene derivatives (6a–c) are confirmed by their spectral data. The characteristic IR absorption bands of compounds (6a–c) prove the presence of NH₂ groups at 3322–2935 cm⁻¹, the cyano groups at 2209–2210 cm⁻¹. Furthermore, the strong bands at

1530–1537 cm^{-1} attribute to the NH bending and the informative bands at 1582–1704 cm^{-1} correspond to the carbonyl groups (ester, pyridone and amide). The ^1H NMR spectra of (6a–c) exhibit the highly deshielded NH protons at the range of $\delta = 9.11$ –10.96 ppm. These findings are supported by similar reported compounds and may be attributed to the tautomerization possibility of 2-pyridone isomeric from the 2-hydroxypyridine form [35]. The NH_2 protons appear in the range of 6.35–6.56 ppm.

2.2. Metal Nanoparticles (MNPs) Characterization

The presence of MNPs was previously confirmed and characterized (c.f. supplementary file S2) [36]. The UV-Vis spectra of the surface plasmon bands appear at 537 and 425 nm, confirming the production of AuNPs and AgNPs, respectively, while disappearance of the absorbance band at 318 nm confirms the production of RuNPs. The high resolution transmittance spectroscopy images (HRTEM) estimate that the sizes of the Au, Ag and Ru nanoparticles with an average diameter of 17, 9 and 5.5 nm, respectively. The results are in good agreement with the literature [37,38].

2.3. Absorption Spectra Analysis

The UV-Vis absorption spectra (A) of the synthesized dyes (6a–c) are measured in DMF (Figure 1), where the values of maximum absorbance wavelengths (λ_{max}) are affected by the strength of the donor in direct proportion. Dye (6b) has a carbonyl group with a stronger accepting character than that of carboxylate and cyano chromophores of (6a) and (6c), respectively; thus, it shows the highest λ_{max} . Since the absorption of D- π -A could be shifted towards longer (λ) (i.e., intramolecular donor and acceptor charge transfer), these dyes may be applied for solar cells [24]. Concurrently, the energy levels could be adjusted by incorporating different anchoring nuclei and the π bridge.

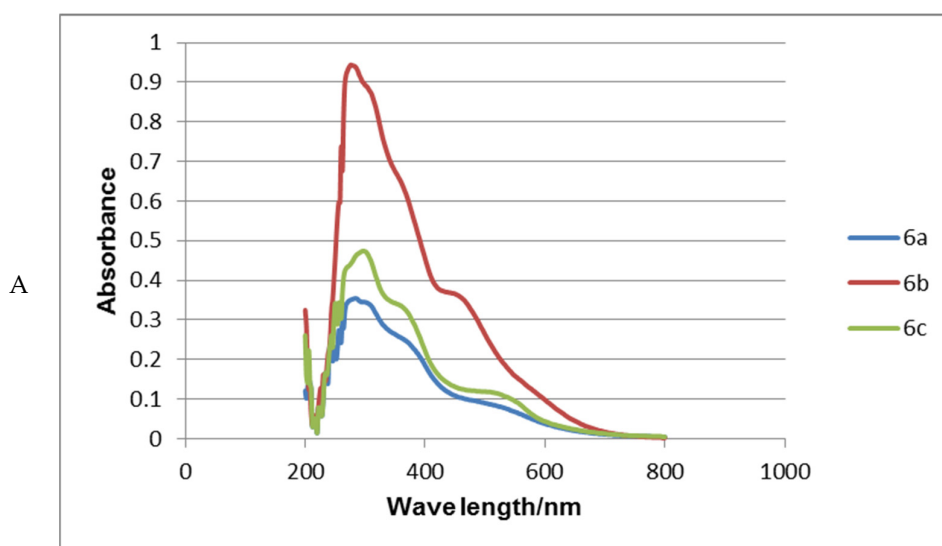


Figure 1. Cont.

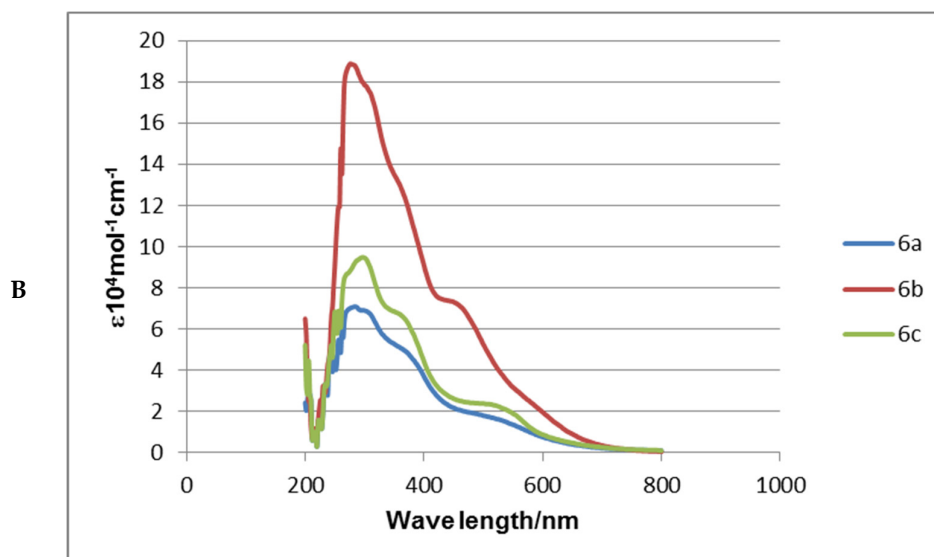


Figure 1. UV-Vis normal absorption spectra (A) and molar absorption coefficients (ϵ) (B) of dyes (6a–c) measured in DMF (5×10^{-2} mM).

According to the light absorption behavior (Figure 2), dye (6b) has the highest adsorption amount on the TiO₂ nanocrystalline surface and hence is chosen to study its performance in conjugation with different metal nanoparticles.

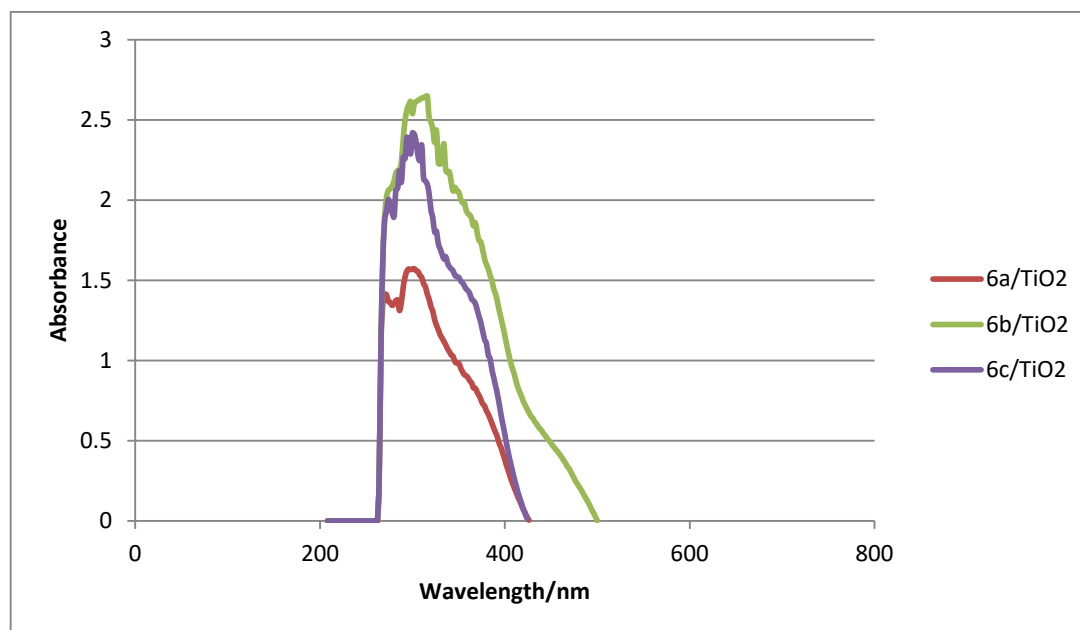


Figure 2. UV-Vis absorption spectra of dyes (6a–c) adsorbed on nanoporous TiO₂.

The adsorbed dye/Au, Ru and/or Ag nanoparticle conjugates (6b/NPs) on nanoporous TiO₂ exhibit the role of their plasmonic resonance phenomena in the enhancement of adsorption efficiency (Figure 3). Generally, the conjugation with nanoparticles shows a slightly higher adsorption amount on the TiO₂ nanocrystalline surface, in the order Ag > Ru > Au, than in the case of dye only.

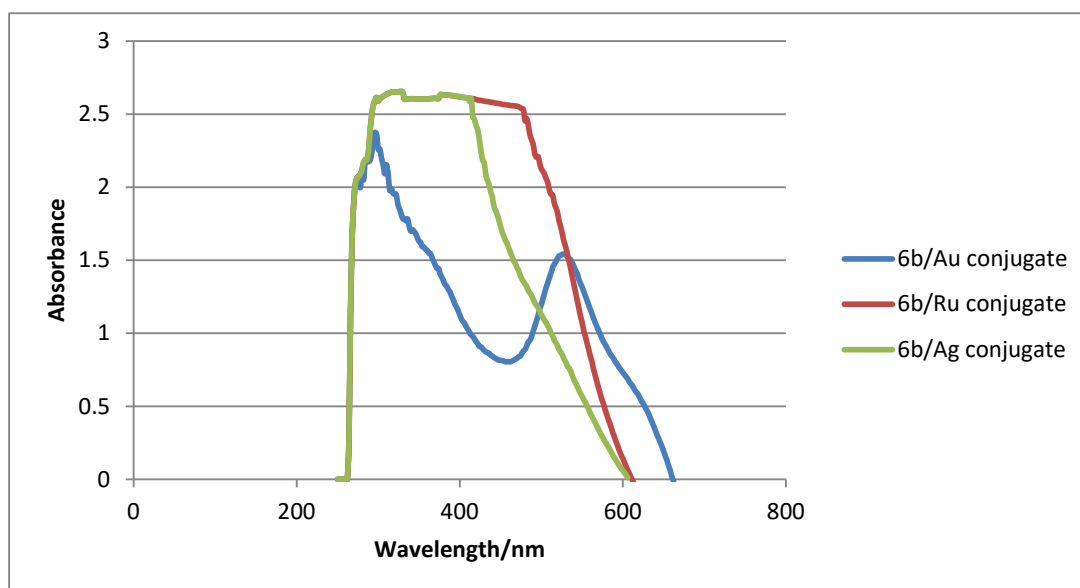


Figure 3. UV-Vis absorption spectra of dye (6b/NPs) conjugates adsorbed on nanoporous TiO₂.

2.4. Electrochemical Characterization

The oxidation and reduction modes corresponding to the removal of electrons from the HOMO and filling the LUMO with electrons, respectively, are determined using cyclic voltammetric measurements [39]. The MO's energy levels are calculated from the onset oxidation and reduction potentials (E_{onset} for HOMO and LUMO, respectively) of cyclic voltammograms (CVs), where the magnitude of their energy gaps (E_g) are estimated.

Figures 4–6 show CVs for dyes (6a–c) in dichloromethane (DCM) with 100 mM tetrabutyl ammonium perchlorate (TBAP) as supporting electrolyte, where a single reversible oxidative wave in a positive potential and an irreversible reductive one in a negative potential appear.

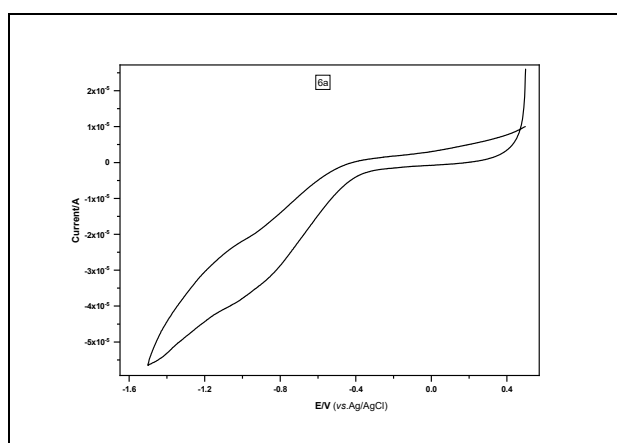


Figure 4. Cyclic voltammogram (CV) of (6a) in dichloromethane (DCM) with tetrabutyl ammonium perchlorate (TBAP).

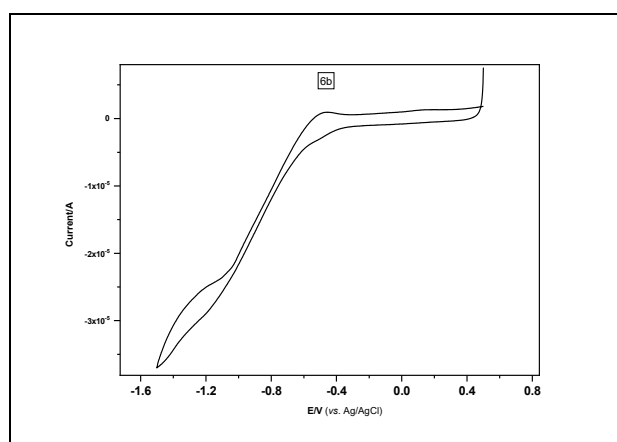


Figure 5. CV of (6b) in DCM with TBAP.

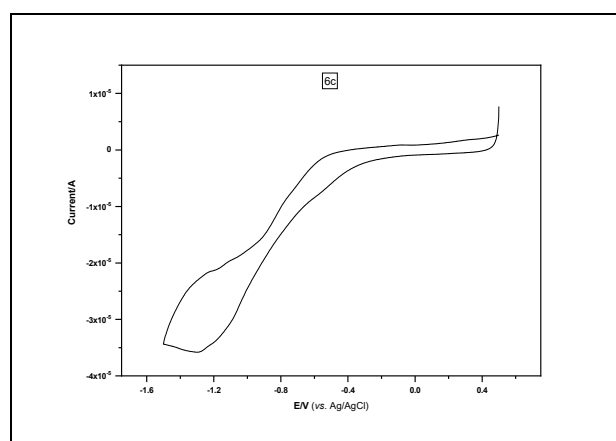


Figure 6. CV of (6c) in DCM with TBAP.

From CV analysis, the E_g for each compound is calculated using the difference between the electrochemical HOMO and LUMO obtained in terms of the optical energy gap of the absorption edge of the electronic spectra (Equations (1) and (2)).

$$E_{HOMO} = -(E_{\text{onst (oxidation)}} + 4.4)\text{eV} \quad (1)$$

$$E_{LUMO} = -(E_{\text{onst (reduction)}} + 4.4)\text{eV} \quad (2)$$

Table 1 obviously shows that dye (6b) has the lowest HOMO-LUMO energy band gap (E_g) among the alternates, indicating the highest performance [40].

Table 1. Electrochemical analysis data of the synthesized dyes (6a–c).

Dye	E_{HOMO} (eV)	E_{LUMO} (eV)	E_g (eV)
6a	−3.30	−3.55	0.25
6b	−3.40	−3.20	0.20
6c	−3.13	−3.73	0.60

Accordingly, dye (6b) is therefore selected to study its performance in conjugation with different metal nanoparticles (i.e., Au, Ag and Ru NPs). The E_g values of (6b/NPs) conjugates are calculated and tabulated in Table 2.

Table 2. Electrochemical analysis data of the synthesized dye (**6b**) conjugated with Au, Ag and Ru NPs.

Dye/MNPs	E _{HOMO} (eV)	E _{LUMO} (eV)	E _g (eV)
6b /AuNPs	−3.10	−3.43	0.33
6b /AgNPs	−3.31	−3.40	0.09
6b /RuNPs	−2.91	−3.43	0.52

Dye (**6b**/AgNPs) has the lowest E_g; thus, the conjugation with silver nanoparticles enhances the efficiency of dye (**6b**) compared with ruthenium and gold conjugates in descending order.

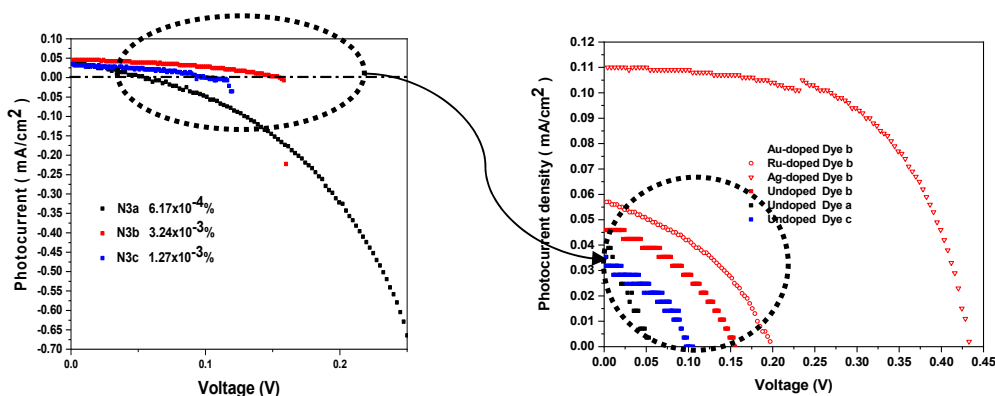
2.5. Photovoltaic Performance (PV) Study

The PV performances of the fabricated DSSC devices using dyes (**6a-c**) along with their NP conjugates on the nanoporous TiO₂ are studied. The PV parameters and characteristic *J-V* curves of the fabricated devices are revealed in Table 3 and Figure 7.

Table 3. *J-V* characteristics of solar devices based on the synthesized dyes (**6a-c**) and (**6b**/NPs) conjugates.

Dye	J _{SC} (mA.cm ^{−2})	V _{OC} (V)	FF	η (%)
6a	4.309 × 10 ^{−2}	0.054	0.27	6.17 × 10 ^{−4}
6b	4.313 × 10 ^{−2}	0.141	0.53	3.24 × 10 ^{−3}
6c	3.243 × 10 ^{−2}	0.102	0.38	1.27 × 10 ^{−3}
6b /Au-NPs	4.065 × 10 ^{−2}	0.182	0.38	2.79 × 10 ^{−3}
6b /Ru-NPs	5.561 × 10 ^{−2}	0.197	0.39	4.16 × 10 ^{−3}
6b /Ag-NPs	1.136 × 10 ^{−1}	0.436	0.57	2.82 × 10 ^{−2}

J_{SC}, short-circuit photocurrent density; V_{OC}, open-circuit photovoltage; FF, fill factor; η, total power conversion efficiency.

**Figure 7.** *J-V* characteristics of the dye-sensitized solar cells (DSSCs) fabricated from dyes (**6a-c**) and (**6b**/NPs) conjugates.

The PV parameters of dyes are in the order **6b** > **6c** > **6a** under the same experimental conditions. The promising results of the J_{SC} values, V_{OC} values and FF values, compared with reported natural and organic sensitizers, may be due to the better interaction between the functional branches of the thiophene nuclei and the surface of the TiO₂ porous film [41]. The cell based on dye (**6b**) exhibits the highest efficiency (J_{SC} = 4.313 × 10^{−2} mA.cm^{−2}, V_{OC} = 0.141 V, FF = 0.53, η = 3.24 × 10^{−3}%) in accordance with the electrochemical measurements. The finding may be explained by the cell's higher adsorption on the TiO₂ nanocrystalline surface among group members, as shown in Figure 2. This phenomenon affords additional absorption sites for the dye, which is correlated with better harvesting efficiency of the photoelectrode, resulting in an improvement in the J_{SC}. The improvement in the open-circuit voltage (V_{OC}) for dye (**6b**) may contribute to an increase of the electron lifetime in

the DSSC by preventing dark current. The increase of the total power conversion efficiency (η) of dye (**6b**) could be ascribed to its better donating ability.

Furthermore, conjugation of the dye molecules with metal nanoparticles exhibits a remarkable change in photovoltaic performance, as described by Table 3 and Figure 7. It's obviously clear that conjugation of dye (**6b**) with silver nanoparticles enhances the efficiency ($\eta = 2.82 \times 10^{-2}\%$) compared with conjugates with Ru and Au in descending order (**6b**/RuNPs; $\eta = 4.16 \times 10^{-3}\%$ and **6b**/AuNPs; $\eta = 2.79 \times 10^{-3}\%$), which could be explained by its higher adsorption on nanoporous TiO₂ (Figure 3).

Overall, the reason for the lower efficiencies of organic sensitizers compared with other metal-based sensitizers may be due to the LUMO level being slightly lower than the energy of the conduction band of TiO₂. This leads to an insufficient electron injection into the TiO₂ conduction band from the excited form of the sensitizers. Many publications have tried to resolve this issue [42] and this will be considered in our future research by modifying the sensitizers' design (i.e., photoanode).

2.6. Computational Study

Quantum chemical calculations are used mainly for geometrical optimization, predicting the Mulliken atomic charges, calculating the frontier molecular orbitals (FMOs) and determining the shape and energy for the compounds under investigation, with the aid of the Gaussian 03W program suite at semi-empirical PM6 level [43]. The geometrical structure is among the important factors governing the chemical and biological activities [44]. The Mulliken atomic charge is also an important factor that affects reactivity towards an electrophilic or nucleophilic reaction [45]. The FMOs are used to find frontier electron density, where the most reactive sites in the molecule are [46].

2.6.1. Molecular Geometry

The dihedral angles data of the DFT-optimized structures indicate the twisted geometry of dyes (**6a–c**) (Table S1 and Figure 8).

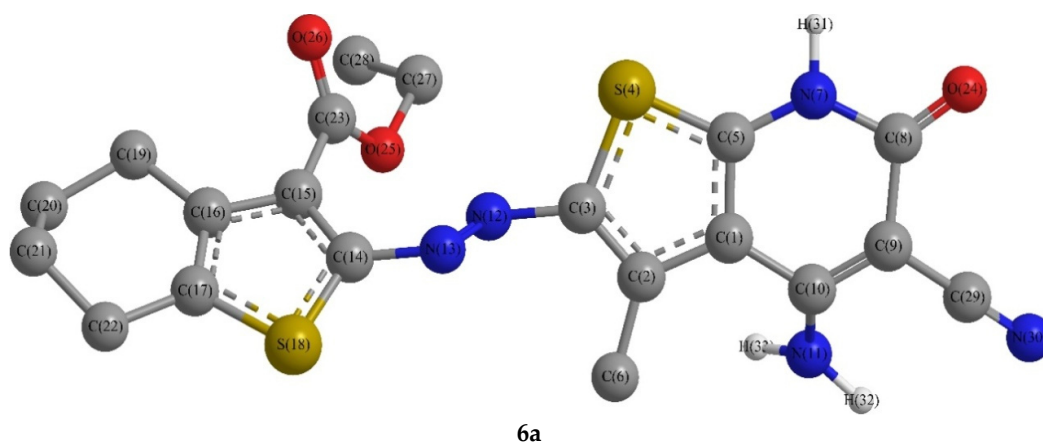


Figure 8. Cont.

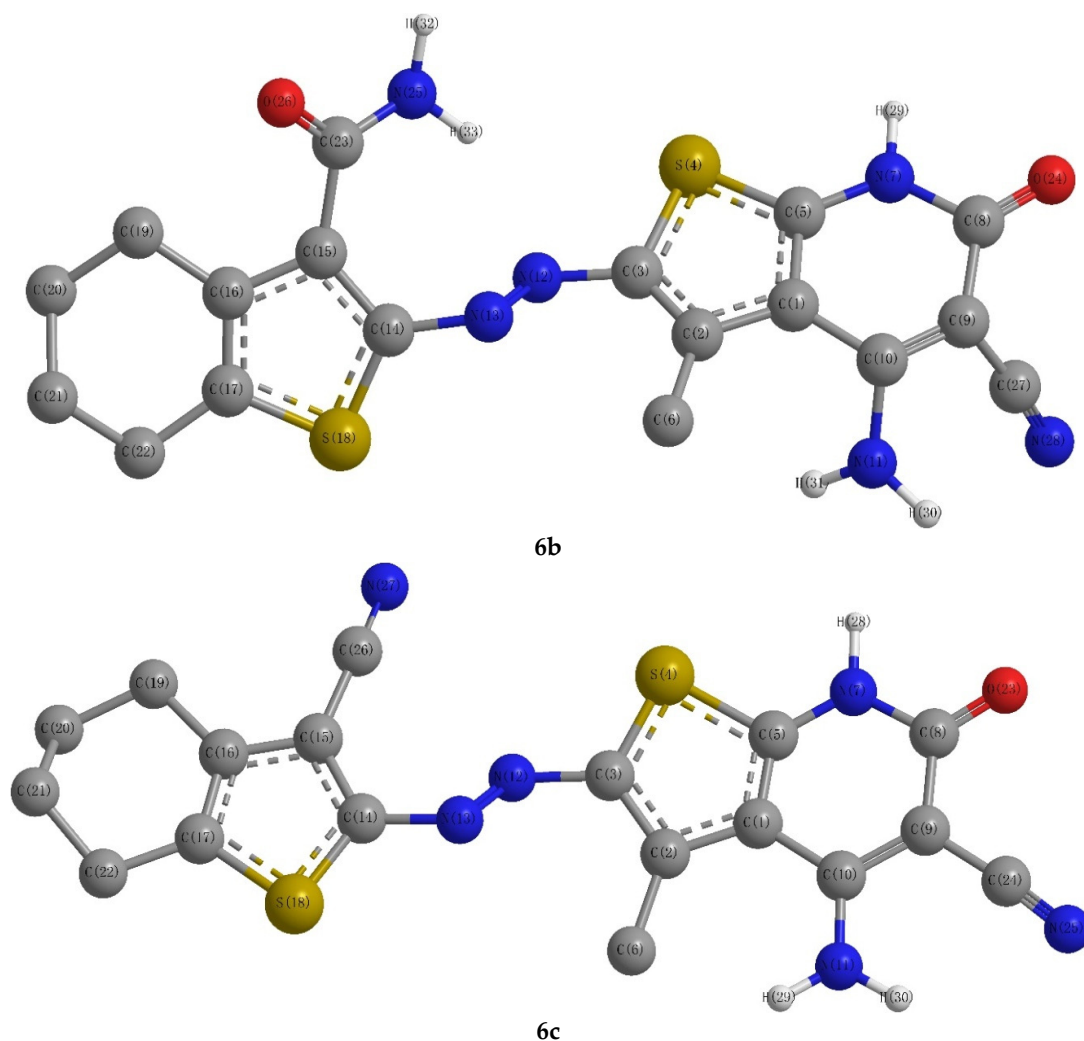


Figure 8. Optimized structures of dyes (6a–c).

For instance, the thiophene rings are almost planar, whereby the S atoms are lying above or below the plane of other C atoms by $\sim 0.5\text{--}6.0^\circ$. The carbon atoms of the thiophene ring fused with pyridine have a distorted planar geometry.

The azo groups are almost planar with the carbon atoms to which they attached, while for the cyclohexyl ring, it is found that both fused moieties are tilted on each other. Moreover, the cyclohexyl rings are bent, and $C_{\text{thio}}\text{--}C_{\text{cyc}}\text{--}C_{\text{cyc}}\text{--}C_{\text{cyc}}$ ranged from 42° to 46° .

Concerning the substituents at 3-position on the cyclohexyl ring fused with thiophene, the carbonyl carbon of COOEt and CONH₂ in the (6a) and (6b) derivatives, in addition to the cyano group carbon in (6c), are almost planar with the thiophene ring. The oxygen atoms of the ester and amide group are found to lie above the thiophene plane by 46.59° and 39.62° , respectively. The cyano and amino substituents on the pyridine ring in the (6a) derivative were on opposite sides, while they were almost planar in (6b) and (6c).

The bond length data, compared with single-crystal X-ray diffraction for peer dyes (Table S2, c.f. supplementary file S1), reveal that the N–N_(azo) bonds are $1.24\text{--}1.25^\circ$, which is in the range reported from the X-ray crystals ($1.18\text{--}1.31 \text{ \AA}$) [47]. Moreover, the DFT $C_{\text{thio}}\text{--}N_{\text{azo}}$ bonds' lengths are in the range 1.41 \AA to 1.47 \AA (X-ray range $1.36\text{--}1.50 \text{ \AA}$) [48]. Furthermore, the range of thiophene C–S bonds' lengths are $1.63\text{--}1.74 \text{ \AA}$ for the cyclohexyl fused rings, while those of fused pyridine are in the range of $1.66\text{--}1.81 \text{ \AA}$, which is in good correlation with the X-ray crystallography data of similar compounds, $1.62\text{--}1.76 \text{ \AA}$ [47].

Finally, the molecular charge distribution is expressed by dipole moment (μ_{total}) and is given as a vector in three dimensions, μ_x , μ_y , and μ_z . Therefore, it can depict the charge movement direction across the molecule depending on the centers of positive and negative charges. For instance, the dipole moments components become zero in symmetric geometrics [49]. The investigated compounds have non-zero components in the Z-direction. This confirms their non-planar structure.

As per dipole moment values (Table 4), dye (6c) is found to be the most polarized among the group members ($\mu_{\text{total}} = 11.54$ Debye), which may be due to the high electron withdrawing character of the cyano group. It has almost a planar structure ($\mu_z = 8.32$ Debye). Accordingly, the investigated compounds may be arranged as **6b** < **6a** < **6c** in polarization characters.

Table 4. Chemical reactivity descriptors (eV) and dipole moment (Debye) of investigated dyes (6a–c).

	6a	6b	6c
E_{HOMO}	−7.23	−7.22	−7.23
E_{LUMO}	−5.29	−5.32	−5.44
ΔE	1.94	1.90	1.79
χ	6.26	6.27	6.34
η	0.97	0.95	0.89
δ	1.03	1.05	1.12
ω	20.17	20.71	22.49
I	7.23	7.22	7.23
A	5.29	5.32	5.44
μ_{total}	10.09	8.32	11.54
μ_x	9.69	−7.82	10.43
μ_y	−1.80	−2.53	−4.93
μ_z	2.16	−1.28	−0.26

2.6.2. Frontier Molecular Orbitals

The energies of the FMOs describe the molecule's ability to donate and accept an electron. They are calculated and presented in Table 4.

The HOMO-LUMO gap (E_g or ΔE) is used for predicting the relationship of the chemical structure and the electronic properties (i.e., frontier electron density and chemical stability) and could explain the ultimate charge transfer across the molecule [50].

The 3D plots of FMOs for the investigated compounds can offer deep perspective about the aromaticity and lone pair (Figure 9) [51]. The positive and negative phases of the wave functions are represented in red and green color, respectively.

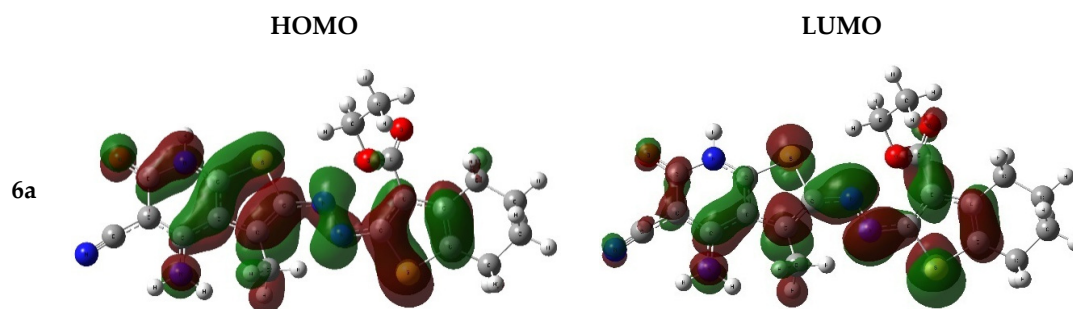


Figure 9. Cont.

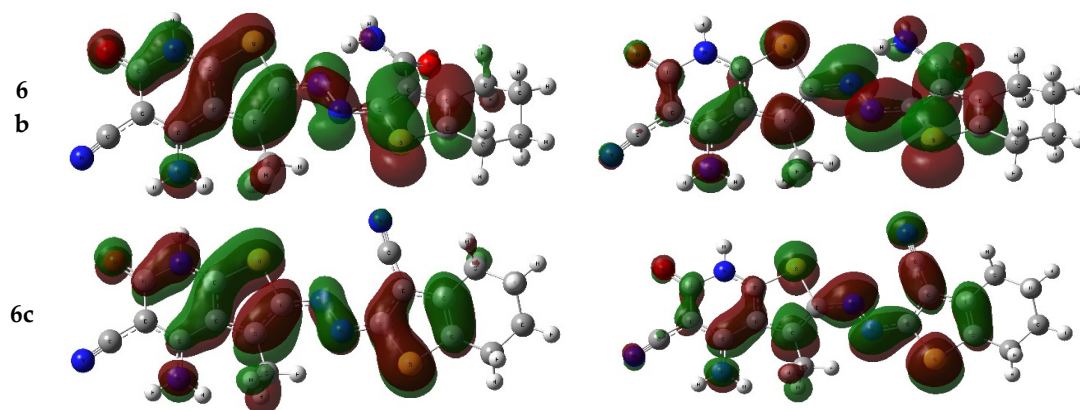


Figure 9. The frontier molecular orbitals (FMOs) of compounds (6a–c).

The HOMO of the (6a–c) derivatives are spread over the whole molecule indicating very small participation for the substituents at position 3 of the thiophene ring fused with the cyclohexyl ring, while the LUMO display strong participation for these groups. The values of energy of both the HOMO and LUMO reflect this effect where the E_{HOMO} data indicate that all compounds have almost the same value, -7.22 eV, while the E_{LUMO} values of the investigated compounds increase gradually and can be ordered as **6a** (-5.25) < **6b** (-5.32) > **6c** (-5.44).

The electronegative groups cause a decrease in the value of E_{LUMO} [52], and therefore, it could be concluded that the cyano group is the most electronegative, while the ester group is the least, in the (6c) and (6a) derivatives, respectively.

The $\Delta E_{\text{HOMO-LUMO}}$ data refer to the highest value of dye (6c), while the (6b) derivative has the lowest, 1.79 and 1.90 eV, respectively. This can be attributed to the increase in the mesomeric effect of substituents on the thiophene ring, which lead to a decrease in the E_g . This enabled molecules to absorb more photons from sunlight beams [53]. Thus, dye (6b) with the lowest ΔE value is probably the most suitable for solar cell application.

2.6.3. Mulliken Atomic Charges

The Mulliken atomic charges data of the investigated compounds show that the nitrogen atoms of the azo group have positive charges (Table S3, c.f. supplementary file S1). The charge value on the S atom of the pyridine ring fused with thiophene, S(18), confirms the high electron withdrawing character of the cyano group at 3-position compared to the amide and ester group, respectively. Moreover, the charge on the oxygen atom of carbonyl, O(26), for the amide group in (6b) and ester group in (6a) may be due to the higher electronegativity of the O than the N atoms, which are adjacent to the carbonyl group.

Fukui function analyses were used for evaluating the most active nucleophilic and electrophilic attack sites (Table S4, c.f. supplementary file S1). Compound (6a) shows that the most susceptible atoms for nucleophilic and electrophilic attacks are almost the same. Moreover, the data of dye (6b) exhibit that the susceptible sites for electrophilic attacks, i.e., electron donation, are S(18), O(26), N(13) and N(12) atoms. Furthermore, dye (6c) analysis shows the susceptible sites for electrophilic or nucleophilic attacks are almost the same but with a different order.

2.6.4. Chemical Reactivity Descriptors

The chemical reactivity descriptors [50] such as electronegativity (χ), global hardness (η), softness (δ), and electrophilicity (ω) are discussed and calculated (c.f. supplementary file S1 and Table 4). As depicted in Table 4, dye (6c) has the higher Lewis acid character (χ), higher hardness (η) and higher electrophilicity index (ω) than the other two derivatives, which are almost equivalent.

3. Materials and Methods

3.1. General

All the chemicals and reagents were analytical grade or chemically pure and were supplied by Sigma Aldrich Co., Darmstadt, Germany. All of the micro, spectral analyses and electrochemical analyses were performed by the Micro Analytical Centers at Taif University, Taif, Saudi Arabia (IR spectra, UV-visible spectra (200–800 nm at RT), TEM and cyclic voltammetry) and at Mansoura University, Mansoura, Egypt (^1H NMR, ^{13}C NMR, MS, HRMS and computational studies). Methodology and instrumentations used were previously reported [54] and are explained in detail in the supplementary file S2.

3.2. Preparation and Characterization of Metal Nanoparticles (MNPs) and their Dye Conjugates

Metal nanoparticles were prepared in our laboratory in dimethyl formamide (DMF) according to the reported methods [36,55]. Characteristics of the synthesized metal nanoparticles (i.e., Au, Ag and Ru) were described in the literature [36,38] (c.f. supplementary file S2). For the preparation of the dyes/metal nanoparticle conjugates, the solid dyes were added to 5 mL of the freshly prepared hot MNPs colloidal solution in DMF. The cooled dye/MNP solutions were characterized using UV-Vis spectrophotometry.

3.3. Electrochemical Analysis

CV measurements were performed using a conventional three electrode cell configuration. Dyes (0.5 mM) were dissolved in DCM with TBAP (100 mM) as supporting electrolyte. CVs were recorded after background subtraction and IR compensation to minimize the double-layer charging current and solution resistance. CV data were measured at scan rate (0.02–5 V/s) in non-aqueous media at $(25 \pm 2)^\circ\text{C}$. All working solutions were thoroughly degassed and the experimental entries were maintained under nitrogen atmosphere. Methodology and instruments are explained in detail in the supplementary file S2.

3.4. Fabrication of Dye-Sensitized Solar Cell (DSSCs) and Photovoltaic Characterizations

Double-layer TiO_2 photoelectrodes ($10 + 5$) μm were prepared and immersed into 0.5 mM of the synthesized compounds (6a–c) in ethanol, for 24 h at room temperature, and the Pt-counter electrodes were also prepared using reported techniques [11,56]. Both electrodes were sealed with 60 mm thick Surlyn (DuPont). Photoelectrochemical tests of the sealed cells were made by illuminating the dye-coated TiO_2 film through the conducting glass support from the anode side with a solar simulator (WXS-155S-10) at AM 1.5 illuminations (light power of 100 mW cm^{-2} , the equivalent of one sun at the surface of test cell). The detailed method is discussed in supplementary file S2.

3.5. Molecular Modeling

Geometrical optimization for the investigated compounds was performed using the Gaussian 09W program suite using the Becke3–Lee–Yang–Parr (B3LYP) exchange-correlation functional with standard 6-311++G (d,p) basis set [57–60]. Methodology and quantum chemical calculations are explained in detail in the supplementary file S1.

3.6. Synthesis and Characterization

3.6.1. Synthesis of 2-amino-3-cyano-4-methylthiophene (1)

The compound was synthesized according to the reported method and found to be in agreement with literature [28]. Pink crystals; yield 95% (10.5 g); m.p.: $120\text{--}121^\circ\text{C}$ (Lit. $118\text{--}119^\circ\text{C}$).

3.6.2. Synthesis of 4-amino-6,7-dihydro-3-methyl-6-oxothieno[2,3-*b*]pyridine-5-carbonitrile (**3**)

A mixture of 2-amino-3-cyano-4-methylthiophene **1** (1.38 g, 10 mmol) and ethyl cyanoacetate (2.26 g, 20 mmol) was refluxed in sodium ethoxide (0.22 g Na/30 mL absolute ethanol, 10 mmol) for 2 h. The reaction mixture was left to cool and then poured onto ice-cold water containing HCl for neutralization. The solid product formed was collected using filtration, dried and recrystallized from ethanol to afford solid brown, yield 77.5% (1.59 g); m.p.: > 250 °C (Lit. > 360 °C [29]).

3.6.3. General Procedure for the Synthesis of 4,5,6,7-tetrahydrobenzo[*b*]thiophenes (**4a–c**)

The cyclohexanone (0.98 g, 10 mmol) was mixed with active nitrile compounds (i.e., (a) ethyl cyanoacetate, 1.13 g; (b) cyanoacetamide, (c) 0.84 g; malononitrile, 0.66 g, 10 mmol), elemental sulfur (0.32 g, 10 mmol) and a catalytic amount of morpholine (2 mL) in ethanol (30 mL), according to the Gewald method [27]. The reaction mixture was then heated at 70 °C in a water bath (WB) for 2 h and left overnight to precipitate. The crystals of (**4a–c**) were collected with good yields and recrystallized from ethanol.

Ethyl 2-amino-4,5,6,7-tetrahydrobenzo[*b*]thiophene-3-carboxylate **4a**. Yellow needles; yield 67% (1.5 g); m.p.: 114–116 °C (Lit. 117–118 °C [61], 116–118 °C [31]).

2-Amino-4,5,6,7-tetrahydrobenzo[*b*]thiophene-3-carboxamide **4b**. Yellowish orange needles; yield 67% (1.5 g); m.p.: 180–181 °C (Lit. 180–181 °C [32], 185 °C [33]).

2-Amino-4,5,6,7-tetrahydrobenzo[*b*]thiophene-3-carbonitrile **4c**. Brown needles; yield 60% (1.1 g); m.p.: 140–142 °C (Lit. 147–148 °C [34]).

3.6.4. General Procedure for Synthesis of thienopyridyl-azo-tetrahydrothiophene Derivatives (**6a–c**)

Molar quantities of thiophenes **4a–c** (2.25 g, 1.96 g, 1.78 g, respectively, 10 mmol) in (3 mL) conc. HCl and (5 mL) of an aqueous NaNO₂ solution (10 mmol, 0.69 g) were mixed and well stirred at 0–5 °C for 30 min. The freshly prepared diazonium salts (**5a–c**) were added afterwards to (20 mL) of ethanolic solution for the coupling of component 2-aminothiazole **1** (2.05 g, 10 mmol) containing sodium acetate (3 g) with slow and continuous stirring at 0–5 °C for 2 h. The resulting products (**6a–c**) were collected, dried and recrystallized from MeOH/Dioxan.

Ethyl(*E*)-2-((4-amino-5-cyano-3-methyl-6-oxo-6,7-dihydrothieno[2,3-*b*]pyridin-2-yl)azo)-4,5,6,7-tetrahydrobenzo[*b*]thiophene-3-carboxylate **6a**. Brown crystals; yield 67.3% (2.96 g); m.p.: 109–110 °C. IR: ν_{\max} = 3322–2936 (N–H_{str.} and NH₂), 2210 (CN), 1704 (CO_{str.-}), 1672 (CO_{str.-}), 1582 (N–H_{bend.}), 1450 (CH₂) and 1396 (CH₃) cm⁻¹; ¹H NMR: δ /ppm = 1.34 (t, *J* = 7.2 Hz, 3H, CH₃), 1.83 (t, *J* = 4.4 Hz, 4H, 2CH₂), 2.43 (s, 3H, CH₃), 2.71 (t, *J* = 4.4 Hz, 2H, CH₂), 2.83 (t, *J* = 4.4 Hz, 2H, CH₂), 4.30 (q, *J* = 7.2 Hz, 2H, CH₂), 6.41 (s, 2H, NH₂) and 9.87 (s, 1H, NH); ¹³C NMR: δ /ppm = 8.2, 13.8, 22.8 (3C), 23.7, 60.4, 79.6, 110.1, 112.6, 115.1, 125.9, 127.3, 129.5, 133.2, 137.4, 159.6, 165.7, 168.1, 173.8; MS (*m/z*, %): 441 (M⁺, 63.4); HRMS calc. for C₂₀H₁₉N₅O₃S₂: 441.0929, found: 441.0911.

(*E*)-2-((4-Amino-5-cyano-3-methyl-6-oxo-6,7-dihydrothieno[2,3-*b*]pyridin-2-yl)azo)-4,5,6,7-tetrahydrobenzo[*b*]thiophene-3-carboxamide **6b**. Reddish brown crystals; yield 96% (3.9 g); m.p.: 172–174 °C. IR: ν_{\max} = 3324–2935 (N–H_{str.} and NH₂), 2209 (CN), 1664 (CO_{str.-}), 1637 (CO_{str.-} amidic), 1582 (N–H_{bend.}), 1449 (CH₂) and 1394 (CH₃) cm⁻¹; ¹H NMR: δ /ppm = 1.83 (t, *J* = 4.4 Hz, 4H, 2CH₂), 2.59 (s, 3H, CH₃), 2.66 (t, *J* = 4.4 Hz, 2H, CH₂), 2.83 (t, *J* = 4.4 Hz, 2H, CH₂), 6.35 (s, 2H, NH₂) 7.81 (s, 2H, NH₂) and 10.96 (s, 1H, NH); ¹³C NMR: δ /ppm = 7.9, 22.9 (2C), 23.1, 24.2, 80.1, 109.8, 113.3, 115.2, 116.4, 124.9, 133.2, 135.4, 138.5, 165.8, 167.5, 168.1, 176.0; MS (*m/z*, %): 412 (M⁺, 25.1); HRMS calc. for C₁₈H₁₆N₆O₂S₂: 412.0776, found: 412.0761.

(*E*)-4-Amino-2-((3-cyano-4,5,6,7-tetrahydrobenzo[*b*]thiophen-2-yl)azo)-3-methyl-6-oxo-6,7-dihydrothieno[2,3-*b*]pyridine-5-carbonitrile **6c**. Dark Brown crystals; yield 74.6% (2.9 g); m.p.: 148–149 °C. IR: ν_{\max} = 3327–2935 (N–H_{str.} and NH₂), 2209 (CN), 1664 (CO_{str.-}), 1582 (N–H_{bend.}), 1448 (CH₂) and 1396 (CH₃) cm⁻¹; ¹H NMR: δ /ppm = 1.73 (t, *J* = 4.4 Hz, 4H, 2CH₂), 2.51 (s, 3H, CH₃), 2.72 (t, *J* = 4.4 Hz, 2H, CH₂), 2.89 (t,

$J = 4.4$ Hz, 2H, CH₂), 6.56 (s, 2H, NH₂) and 9.11 (s, 1H, NH); ¹³C NMR: δ /ppm = 8.1, 22.7 (2C), 23.4, 23.9, 81.0, 102.3, 110.1, 113.5, 114.9, 115.2, 133.5, 134.1, 135.1, 140.3, 166.0, 167.8, 176.0; MS (m/z , %): 394 (M⁺, 13.1); HRMS calc. for C₁₈H₁₄N₆OS₂: 394.0671, found: 394.0660.

4. Conclusions

Our work demonstrates that the introduction of a substituted thiophene segment is of great benefit as a D- π -A organic sensitizer for solar cell applications. Thus, three novel diazenyl pyridothiophene derivatives (**6a–c**) were synthesized as the result of the diazo coupling reaction of 2-amino-4,5,6,7-tetrahydrobenzo[*b*]thiophenes (**4a–c**) with 4-amino-6,7-dihydro-3-methyl-6-oxothieno[2,3-*b*]pyridine-5-carbonitrile (**3**). Their chemical structures are established on the basis of their spectral data. The substituent groups (i.e., COOEt, CONH₂ and CN) are conjugated with the whole molecule, leading to light-harvesting capability of the dye and, more importantly, quite a smooth electron injection process. The effect of the anchoring groups is studied based on the band gap energy (E_g) of their FMOs. Spectroscopy and electrochemical analysis confirmed that the keto acceptor of dye (**6b**) is a relatively stronger acceptor and improved the photovoltaic performance compared with other substituents. The modeling study is in good agreement with the practical findings. Plasmon resonance employing noble metals (i.e., gold, silver and ruthenium) has been recently introduced to the DSSCs using electrostatic interaction with the synthesized diazenyl thieno-pyridyl dyes, where the localized surface plasmon resonance phenomena of metal nanoparticles enhance the light harvesting efficiency. The conjugation with silver nanoparticles (**6b**/AgNPs) exhibits the best results over the studied alternatives. This finding is supported by the data measured and calculated of the HOMO-LUMO band gap energy. The introduction of stronger accepting and donating groups and increasing the planarity of the system using a triple bond bridge will provide a powerful strategy for the development of thiophene based highly efficient D- π -A organic sensitizer in the future.

Supplementary Materials: The following are available online, Modeling S1: Modeling study, Experimental S2: Experimental.

Author Contributions: M.E.K. and A.S.A.A. conceived and designed the chemical experiments, performed the experiments, analyzed the data, contributed reagents/materials/analysis tools and wrote the paper. G.A.M.M. designed, supervised and performed the electrochemical experiments. A.M. designed, supervised and performed the solar energy experiments. All authors have read and agreed to the published version of the manuscript.

Funding: This research received no external funding.

Conflicts of Interest: The authors declare no conflicts of interest.

References

1. O'Regan, B.; Grätzel, M. A low-cost, high-efficiency solar cell based on dye-sensitized colloidal TiO₂ films. *Nature* **1991**, *353*, 737–740. [[CrossRef](#)]
2. Zhou, N.; Prabakaran, K.; Lee, B.; Chang, S.H.; Harutyunyan, B.; Guo, P.; Butler, M.R.; Timalina, A.; Bedzyk, M.J.; Ratner, M.A.; et al. Metal-Free Tetrathienoacene Sensitizers for High-Performance Dye-Sensitized Solar Cells. *J. Am. Chem. Soc.* **2015**, *137*, 4414–4423. [[CrossRef](#)] [[PubMed](#)]
3. Lee, C.-P.; Li, C.-T.; Ho, K.-C. Use of organic materials in dye-sensitized solar cells. *Mater. Today* **2017**, *20*, 267–283. [[CrossRef](#)]
4. Mishra, A.; Fischer, M.K.R.; Bäuerle, P. Metal-Free Organic Dyes for Dye-Sensitized Solar Cells: From Structure: Property Relationships to Design Rules. *Angew. Chem. Int.* **2009**, *48*, 2474–2499. [[CrossRef](#)]
5. Batista, R.M.; Oliveira, E.; Nuñez, C.; Costa, S.P.; Lodeiro, C.; Raposo, M.M.M. Synthesis and evaluation of new thienyl and bithienyl-bis-indolylmethanes as colorimetric sensors for anions. *J. Phys. Org. Chem.* **2009**, *22*, 362–366. [[CrossRef](#)]
6. Ahmad, S.; Guillén, E.; Kavan, L.; Grätzel, M.; Nazeeruddin, M.K. Metal free sensitizer and catalyst for dye sensitized solar cells. *Energy Environ. Sci.* **2013**, *6*, 3439–3466. [[CrossRef](#)]

7. Eom, Y.K.; Hong, J.Y.; Kim, J.; Kim, H.K. Triphenylamine-based organic sensitizers with π -spacer structural engineering for dye-sensitized solar cells: Synthesis, theoretical calculations, molecular spectroscopy and structure-property-performance relationships. *Dyes Pigm.* **2017**, *136*, 496–504. [[CrossRef](#)]
8. Obotowo, I.N.; Obot, I.B.; Ekpe, U.J. Organic sensitizers for dye-sensitized solar cell (DSSC): Properties from computation, progress and future perspectives. *J. Mol. Struct.* **2016**, *1122*, 80–87. [[CrossRef](#)]
9. Wu, X.; Lu, G.Q.; Wang, L. Shell-in-shell TiO₂ hollow spheres synthesized by one-pot hydrothermal method for dye-sensitized solar cell application. *Energy Environ. Sci.* **2011**, *4*, 3565–3572. [[CrossRef](#)]
10. Kavan, L. Electrochemistry and dye-sensitized solar cells. *Curr. Opin. Electrochem.* **2017**, *2*, 88–96. [[CrossRef](#)]
11. Ito, S.; Chen, P.; Comte, P.; Nazeeruddin, M.K.; Liska, P.; Péchy, P.; Grätzel, M. Fabrication of screen-printing pastes from TiO₂ powders for dye-sensitized solar cells. *Prog. Photovolt. Res. Appl.* **2007**, *15*, 603–612. [[CrossRef](#)]
12. Batista, R.M.F.; Costa, S.P.G.; Belsley, M.; Raposo, M.M.M. Synthesis and optical properties of novel, thermally stable phenanthrolines bearing an arylthienyl-imidazo conjugation pathway. *Dyes Pigm.* **2009**, *80*, 329–336. [[CrossRef](#)]
13. Genin, E.; Hugues, V.; Clermont, G.; Herbivo, C.; Castro, M.C.R.; Comel, A.; Raposo, M.M.M.; Blanchard-Desce, M. Fluorescence and two-photon absorption of push-pull aryl (bi) thiophenes: Structure-property relationships. *Photochem. Photobiol. Sci.* **2012**, *11*, 1756–1766. [[CrossRef](#)]
14. Raposo, M.M.M.; Kirsch, G. Formylation, dicyanovinylolation and tricyanovinylolation of 5-alkoxy-and 5-amino-substituted 2, 2'-bithiophenes. *Tetrahedron* **2003**, *59*, 4891–4899. [[CrossRef](#)]
15. Ishikawa, K.; Wen, C.-J.; Yamada, K.; Okubo, T. The Photocurrent of Dye-Sensitized Solar Cells Enhanced by the Surface Plasmon Resonance. *J. Chem. Eng. Jpn.* **2004**, *37*, 645–649. [[CrossRef](#)]
16. Kim, H.-Y.; Song, D.H.; Yoon, H.; Suh, J.S. Surface plasmon-enhanced dye-sensitized solar cells based on double-layered composite films consisting of TiO₂/Ag and TiO₂/Au nanoparticles. *RSC Adv.* **2015**, *5*, 27464–27469. [[CrossRef](#)]
17. Neese, F. Prediction of molecular properties and molecular spectroscopy with density functional theory: From fundamental theory to exchange-coupling. *Coord. Chem. Rev.* **2009**, *253*, 526–563. [[CrossRef](#)]
18. Nafee, S.S.; Hagar, M.; Ahmed, H.A.; Alhaddad, O.A.; El-Shishtawy, R.M.; Raffah, B.M. New two rings Schiff base liquid crystals; ball mill synthesis, mesomorphic, Hammett and DFT studies. *J. Mol. Liq.* **2020**, *299*, 112161. [[CrossRef](#)]
19. Nafee, S.S.; Hagar, M.; Ahmed, H.A.; El-Shishtawy, R.M.; Raffah, B.M. The synthesis of new thermal stable schiff base/ester liquid crystals: A computational, mesomorphic, and optical study. *Molecules* **2019**, *24*, 3032. [[CrossRef](#)]
20. Zajac, A.; Dymińska, L.; Lorenc, J.; Ptak, M.; Hanuza, J. Syntheses, spectroscopic properties and molecular structure of silver phytate complexes-IR, UV-VIS studies and DFT calculations. *J. Mol. Struct.* **2018**, *1156*, 483–491. [[CrossRef](#)]
21. Ramesh, G.; Reddy, B.V. Spectroscopic investigation on structure (monomer and dimer), molecular characteristics and comparative study on vibrational analysis of picolinic and isonicotinic acids using experimental and theoretical (DFT & IVP) methods. *J. Mol. Struct.* **2018**, *1160*, 271–292.
22. Orief, M.I.; Abdel-Rhman, M.H. Molecular modeling, spectroscopic and structural studies on newly synthesized ligand N-benzoyl-2-isonicotinoylhydrazine-1-carboxamide. *J. Mol. Struct.* **2018**. [[CrossRef](#)]
23. Khalifa, M.; Abdel-Latif, E.; Gobouri, A. Disperse Dyes Based on 5-Arylazo-thiazol-2-ylcarbamoyl-thiophenes: Synthesis, Antimicrobial Activity and Their Application on Polyester. *J. Heterocycl. Chem.* **2015**, *52*, 674–680. [[CrossRef](#)]
24. Khalifa, M.E.; Al-Amoudi, M.S.; Gobouri, A.A.; Merazga, A.; Fadda, A.A. Synthesis of Novel Arylazothiazolyl-thiophene Dyes for Solar Cell and Nonlinear Optical Materials. *Acta Chim. Slov.* **2015**, *63*, 121–128. [[CrossRef](#)] [[PubMed](#)]
25. Al-Baradi, A.M.; Al-Shehri, W.A.; Badawi, A.; Almalki, A.S.A.; Merazga, A. A study of the nanostructure and efficiency of solid-state dye-sensitized solar cells based on a conducting polymer. *Heliyon* **2019**, *5*, e01472. [[CrossRef](#)]
26. Almalki, A.S.A.; Alhadhrami, A.; Obaid, R.J.; Alsharif, M.A.; Adam, A.M.A.; Grabchev, I.; Refat, M.S. Preparation of some compounds and study their thermal stability for use in dye sensitized solar cells. *J. Mol. Liq.* **2018**, *261*, 565–582. [[CrossRef](#)]
27. Gewald, K. Zur Reaktion von α -Oxo-mercaptanen mit Nitrilen. *Angew. Chem.* **1961**, *73*, 114. [[CrossRef](#)]

28. Pak, F.; Ekinçi, D.; Tümer, F.; Demir, Ü. A Mechanistic and Characteristic Investigation of Electrooxidation of 2-Amino-3-cyano-4-methylthiophene. *Macromol. Chem. Phys.* **2007**, *208*, 2367–2374. [[CrossRef](#)]
29. Gewald, K.; Schäfer, H.; Sattler, K. Synthesen von 4-Amino-thieno[2,3-*b*]pyridinen. *Monatsh. Chem.* **1979**, *110*, 1189–1196. [[CrossRef](#)]
30. Baron, H.; Remfry, F.G.P.; Thorpe, J.F. The formation and reactions of imino-compounds. Part I. Condensation of ethyl cyanoacetate with its sodium derivative. *J. Chem. Soc. Trans.* **1904**, *85*, 1726–1761. [[CrossRef](#)]
31. Csukonyi, K.; Lázár, J.; Bernáth, G.; Hermecz, I.; Mészáros, Z. Saturated heterocycles, 75. Preparation of tetracyclic thiophene derivatives with bridgehead nitrogen. Synthesis of polymethylenethieno [2, 3-*d*] dihydropyrrolo-, tetrahydropyrrolo- and tetrahydroazepino [1, 2-*a*] pyrimidin-4-ones and-4-thiones. *Monatsh. Chem.* **1986**, *117*, 1295–1303. [[CrossRef](#)]
32. Perrissin, M.; Favre, M.; Luu-Duc, C.; Bakri-Logeais, F.; Huguet, F.; Narcisse, G. Thieno (2,3-*d*)-4-pyrimidones: Synthesis, structure and pharmacological properties. *Eur. J. Med. Chem.* **1984**, *19*, 420–424.
33. Offermann, W.; Eger, K.; Roth, H.J. Synthesen bicyclischer 1, 2, 6-Thiadiazine. *Arch. Pharm.* **1981**, *314*, 168–175. [[CrossRef](#)]
34. Amr, A.E.-G.E.; Sherif, M.H.; Assy, M.G.; Al-Omar, M.A.; Ragab, I. Antiarrhythmic, serotonin antagonist and antianxiety activities of novel substituted thiophene derivatives synthesized from 2-amino-4, 5, 6, 7-tetrahydro-*N*-phenylbenzo [*b*] thiophene-3-carboxamide. *Eur. J. Med. Chem.* **2010**, *45*, 5935–5942. [[CrossRef](#)]
35. Maruoka, H.; Yamagata, K.; Yamazaki, M. Studies on Heterocyclic Enaminonitriles, XV. A Convenient One-pot Synthesis of Ethyl 4-Amino-2, 3-dihydrothieno-[2, 3-*b*] pyridine-5-carboxylates. *Liebigs Ann. Chem.* **1993**, *1993*, 1269–1271. [[CrossRef](#)]
36. Khalifa, M.E.; Elkhawass, E.A.; Pardede, A.; Ninomiya, M.; Tanaka, K.; Koketsu, M. A facile synthesis of formazan dyes conjugated with plasmonic nanoparticles as photosensitizers in photodynamic therapy against leukemia cell line. *Monatsh. Chem.* **2018**, *149*, 2195–2206. [[CrossRef](#)]
37. Chauhan, A.; Zubair, S.; Tufail, S.; Sherwani, A.; Sajid, M.; Raman, S.C.; Azam, A.; Owais, M. Fungus-mediated biological synthesis of gold nanoparticles: Potential in detection of liver cancer. *Int. J. Nanomedicine* **2011**, *6*, 2305–2319.
38. Kusada, K.; Kobayashi, H.; Yamamoto, T.; Matsumura, S.; Sumi, N.; Sato, K.; Nagaoka, K.; Kubota, Y.; Kitagawa, H. Discovery of Face-Centered-Cubic Ruthenium Nanoparticles: Facile Size-Controlled Synthesis Using the Chemical Reduction Method. *J. Am. Chem. Soc.* **2013**, *135*, 5493–5496. [[CrossRef](#)]
39. Asiri, A.M.; Khan, S.A. Synthesis, characterization and optical properties of mono- and bis-chalcone. *Mater. Lett.* **2011**, *65*, 1749–1752. [[CrossRef](#)]
40. Kong, Z.; Liu, D.; He, J.; Wang, X. Electrode buffer layers producing high performance nonvolatile organic write-once-read-many-times memory devices. *RSC Adv.* **2017**, *7*, 13171–13176. [[CrossRef](#)]
41. Yu, Q.; Liu, S.; Zhang, M.; Cai, N.; Wang, Y.; Wang, P. An Extremely High Molar Extinction Coefficient Ruthenium Sensitizer in Dye-Sensitized Solar Cells: The Effects of π -Conjugation Extension. *J. Phys. Chem. C* **2009**, *113*, 14559–14566. [[CrossRef](#)]
42. Bonomo, M.; Carella, A.; Borbone, F.; Rosato, L.; Dini, D.; Gontrani, L. New pyran-based molecules as both n- and p-type sensitizers in semi-transparent Dye Sensitized Solar Cells. *Dyes Pigm.* **2020**, *175*, 108140. [[CrossRef](#)]
43. Dennington, R.; Keith, T.; Millam, J. *GaussView*, 5th ed.; Semichem Inc.: Shawnee, KS, USA, 2009.
44. Karelson, M.; Lobanov, V.S.; Katritzky, A.R. Quantum-chemical descriptors in QSAR/QSPR studies. *Chem. Rev.* **1996**, *96*, 1027–1044. [[CrossRef](#)] [[PubMed](#)]
45. Domingo, L.R.; Pérez, P.; Sáez, J.A. Understanding the local reactivity in polar organic reactions through electrophilic and nucleophilic Parr functions. *RSC Adv.* **2013**, *3*, 1486–1494. [[CrossRef](#)]
46. Fukui, K.; Yonezawa, T.; Shingu, H. A molecular orbital theory of reactivity in aromatic hydrocarbons. *J. Chem. Phys.* **1952**, *20*, 722–725. [[CrossRef](#)]
47. Chen, H.; Liu, M.-G. Synthesis, characterization and crystal structure of heterocyclic tetrahydropyrrolo [4', 3': 4, 5] thieno [2, 3-*d*] pyrimidinone derivatives via sequential aza-Wittig/base catalyzed cyclization. *J. Mol. Struct.* **2019**, *1180*, 31–40. [[CrossRef](#)]
48. Khojasteh, V.; Kakanejadifard, A.; Zabardasti, A.; Azarban, F. Spectral, structural, solvatochromism, biological and computational investigation of some new azo-azomethines containing N-alkylpyridinium salts. *J. Mol. Struct.* **2019**, *1175*, 261–268. [[CrossRef](#)]

49. Datta, A. Role of metal ions (M= Li⁺, Na⁺, and K⁺) and pore sizes (Crown-4, Crown-5, and Crown-6) on linear and nonlinear optical properties: New materials for optical birefringence. *J. Phys. Chem. C* **2009**, *113*, 3339–3344. [[CrossRef](#)]
50. Xavier, S.; Periandy, S.; Ramalingam, S. NBO, conformational, NLO, HOMO–LUMO, NMR and electronic spectral study on 1-phenyl-1-propanol by quantum computational methods. *Spectrochim. Acta A* **2015**, *137*, 306–320. [[CrossRef](#)]
51. Arjunan, V.; Balamourougane, P.; Kalaivani, M.; Raj, A.; Mohan, S. Experimental and theoretical quantum chemical investigations of 8-hydroxy-5-nitroquinoline. *Spectrochim. Acta A* **2012**, *96*, 506–516. [[CrossRef](#)]
52. Amorim, R.; de Meneses, M.D.F.; Borges, J.C.; da Silva Pinheiro, L.C.; Caldas, L.A.; Cirne-Santos, C.C.; de Mello, M.V.P.; de Souza, A.M.T.; Castro, H.C.; de Palmer Paixao, I.C.N. Thieno [2, 3-b] pyridine derivatives: A new class of antiviral drugs against Mayaro virus. *Arch. Virol.* **2017**, *162*, 1577–1587. [[CrossRef](#)] [[PubMed](#)]
53. Tayfuroğlu, Ö.; Kılıçarslan, F.A.; Atmaca, G.Y.; Erdoğan, A. Synthesis, characterization of new phthalocyanines and investigation of photophysical, photochemical properties and theoretical studies. *J. Porphyr. Phthalocyanines* **2018**, *22*, 250–265. [[CrossRef](#)]
54. Khalifa, M.; Gobouri, A.; Kabli, F.; Altalhi, T.; Almalki, A.; Mohamed, M. Synthesis, Antibacterial, and Anti HepG2 Cell Line Human Hepatocyte Carcinoma Activity of Some New Potentially Benzimidazole-5-(Aryldiazenyl)Thiazole Derivatives. *Molecules* **2018**, *23*, 3285. [[CrossRef](#)] [[PubMed](#)]
55. Chen, Y.; Liew, K.Y.; Li, J. Size-controlled synthesis of Ru nanoparticles by ethylene glycol reduction. *Mater. Lett.* **2008**, *62*, 1018–1021. [[CrossRef](#)]
56. Perdew, J.P.; Burke, K.; Ernzerhof, M. Generalized Gradient Approximation Made Simple. *Phys. Rev. Lett.* **1996**, *77*, 3865–3868. [[CrossRef](#)]
57. Frisch, M.; Trucks, G.; Schlegel, H.; Scuseria, G.; Robb, M.; Cheeseman, J.; Scalmani, G.; Barone, V.; Mennucci, B.; Petersson, G. *Gaussian 09, Revision, A.1*; Gaussian: Wallingford, CT, USA, 2009.
58. Becke, A.D. Density-functional thermochemistry. III. The role of exact exchange. *J. Chem. Phys.* **1993**, *98*, 5648–5652. [[CrossRef](#)]
59. Lee, C.; Yang, W.; Parr, R.G. Development of the Colle-Salvetti correlation-energy formula into a functional of the electron density. *Phys. Rev. B* **1988**, *37*, 785. [[CrossRef](#)]
60. Perdew, J.P.; Wang, Y. Pair-distribution function and its coupling-constant average for the spin-polarized electron gas. *Phys. Rev. B* **1992**, *46*, 12947. [[CrossRef](#)]
61. Fondjo, E.S.; Döpp, D.; Henkel, G. Reactions of some anellated 2-aminothiophenes with electron poor acetylenes. *Tetrahedron* **2006**, *62*, 7121–7131. [[CrossRef](#)]

Sample Availability: Samples of the compounds(6a–c) are available from the authors.



© 2020 by the authors. Licensee MDPI, Basel, Switzerland. This article is an open access article distributed under the terms and conditions of the Creative Commons Attribution (CC BY) license (<http://creativecommons.org/licenses/by/4.0/>).